

IMECE2006-15174

## NUMERICAL MODELING OF EM PUMP EFFICIENCY

Daniel P. Cook<sup>1</sup>  
dpcook@me.unlv.edu

Yitung Chen<sup>1</sup>  
uuchen@nscee.edu

Lillian J. Ratliff<sup>2</sup>  
ratliff@student.egr.unlv.edu

Huajun Chen<sup>1</sup>  
huajunc@nscee.edu

Jian Ma<sup>1</sup>  
jianma@egr.unlv.edu

<sup>1</sup> Department of Mechanical Engineering, University of Nevada, Las Vegas, Nevada, 89154, US

<sup>2</sup> Department of Electrical Engineering, University of Nevada, Las Vegas, Nevada, 89154, US

### ABSTRACT

The pilot Molten lead-bismuth target circuit (TC-1) in University of Nevada, Las Vegas (UNLV) was designed for beam power of 1 MW accelerator driven system (ADS). The TC-1 is a liquid lead-bismuth eutectic (LBE) circulation loop. Circulation of the liquid alloy is driven by an annular linear induction pump (ALIP). Experimental measurements of system parameters have yielded a surprisingly low pump efficiency of less than 1%. A numerical study of the pump efficiency has been conducted to determine which operational parameters are responsible for this low efficiency and to give insight into future EM pump design. The numerical study has entailed incorporating algorithms which calculated the EM body force into a commercial CFD code (FEMLab). The EM body forces were calculated using both simplified analytic expressions, as well as by numerical solution of Maxwell's equations.

### INTRODUCTION

Electromagnetic (EM) pumps have been used in metal refinery, or liquid metal cooled nuclear reactors for transporting heat. Such pumps are attractive because of their advantages to obtain hermetically sealed systems over conventional mechanical pumps, although their efficiency is quite weak. The pumping force in an EM pump does not come from a piston or an impeller moving in the liquid. Instead, force is

exerted on the liquid metal, which is a conductor of electricity. Because there is absence of sealings, bearings and moving parts in EM pump, low maintenance cost is required [1]. In addition, their various advantages can also be found in low degradation rate of the structure material, simple replacement of the inductor without cut of the piping system, fine regulation of flow rate by different inductor connections and pump characteristics easy changing without change of the mechanical set-up.

The EM pumps are used for a wide range of liquid metals, such as lead, lead alloy, lithium, sodium, sodium-potassium alloy, magnesium, mercury, gallium, alkali metals, molten steel and others [2]. Recently, EM pump can also be found in the application of micro-fluidics and micro-fluidic devices [3, 4].

According to specification for different applications, the EM pump can be principally classified as conduction and induction pump. Alternative current (AC) and direct current (DC) of the power feed into EM pump is another classifications. In the AC linear induction pump design, there are flat linear induction pump (FLIP), annular linear induction pump (ALIP) and helical induction pump according to their winding construction [2].

In the FLIPs, the pump duct is a flattened tube that passes through the gap between two stators. Apart from FLIPs, the ALIPs can be obtained by rerolling the winding of flat linear induction around the direction of motion. The duct containing the liquid metal is an annulus. The stator windings are in the form of flat "pancake" coils [2, 5]. In the helical induction

pump, the stator or magnetic field source is identical to the stator of a three-phase asynchronous induction motor. The helical induction pump was chosen for the specification of high pressure and relatively low flow rate. The duct is made in helical form to decrease the active length. The axial component of fluid velocity results in additional loss and reduction in outlet of pump due to this design. However this effect is insignificant in pumps with a small helix angle.

On the other hand, the permanent magnet pump generate alternating traveling magnetic field by rotating permanent magnet with alternating polarity fixed on solid ferrous base. It is a much simpler construction design with smaller overall dimensions of active part and weight due to no winding at all. Different from permanent magnet pumps, the FLIPs, ALIPs, and helical induction pumps all have stationary magnetic structures. This design advantage can be found in certain applications. For example, in space vehicles, the presence of rotating components might pose guidance problems [2].

The ALIPs have been used and studied in R&D facilities in support of the development of advanced nuclear reactors and waste transmutation target systems. In University of Nevada, Las Vegas, one ALIP is the prime mover in the pilot molten lead-bismuth eutectic (LBE) target circuit TC-1 that is designed in Russia (IPPE, Obninsk, ISTC#559) to accommodate an 800 MeV proton beam power of 1 MW. Under the rated pressure of 0.102 MPa in TC-1, the pump's capacity is 15 m<sup>3</sup>/h. However, its efficiency is very weak below 1% [6].

Furthermore, the ALIPs in the facility of LBE cooled target within the MegaWatt Pilot Experiment (MEGAPIE) project have similar low efficiencies. The main pump is tandem aligned with a bypass pump. The efficiencies for main and bypass pump are only 1.18% and 0.249%, respectively [7].

The reducing of pump efficiency is due to the power loss in ohmic loss in winding, shot-cur core, tube wall, slip and hydraulic loss, eddy current loss, hysteresis losses and end effect etc [2].

In contrast to rotary induction machine, linear induction machines have open magnetic structure along the direction of motion. Therefore, additional phenomena called end effects occur due to this design [5]. The magnetic field in an ALIP has a strong stationary alternating component at each end resulting from the discontinuous stator laminations at the ends. This produces eddy-current braking losses beyond those produced by the entry and exit of the liquid metal (end losses).

The longitudinal end effect in linear induction pumps results in the developed pressure decrease and in arising of pressure pulsation with double frequency of the power supply source [8].

The end effect of the pulsating component of the flux is to add a pulsating component of the current in the liquid metal, which performs no useful work but increases the ohmic losses by a factor  $(1+s^2)/s^2$  and lower the efficiency by a factor  $s/(1+s)$ . Where the slip  $s$  is defined by the difference between fluid velocity  $v_f$  and the magnetic field synchronous velocity  $v_B$  divided by  $v_B$ , as  $s = (v_B - v_f) / v_B$  [9].

Double-supply-frequency pressure pulsation and the magnetohydrodynamic instability in ALIP were studied experimentally and analytically [8, 10]. A two-dimensional model for analysis of ALIP (or cylindrical linear induction pump) was employed to study the hydraulic performance [9, 11].

In this work, both of theoretical and numerical methods are used to evaluate the TC-1 pump performance. The theoretical method, which is based on equivalent current sheet model and developed by Cho and Hong[12], was applied to our current pump. The commercial software package, Comsol 3.2, is used for the numerical simulation. Comparison with numerical and theoretical results was made to benchmark the models.

## THE ANALYTIC EM MODEL

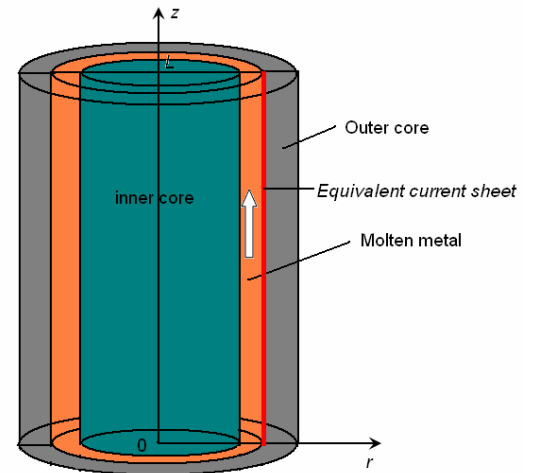


Fig.1 Schematic of an annular-type linear induction electromagnetic pump

In EM induction pumps, a 3-phase, sinusoidally varying excitation current running through the primary coils in the outer core, produces a traveling magnetic field, as shown in Fig.1. This magnetic field in turn induces electrical currents in the liquid metal in the pump. The interaction of the magnetic field and the induced currents produces an EM body force responsible for propelling the liquid metal. One way to simplify the modeling of these types of pumps is to replace the currents running in the discrete primary coils with an equivalent current sheet, which is located at the boundary between the liquid

metal and the outer core. The current sheet only has a component in the  $\theta$ -direction and can be expressed as:

$$J_s(z, t) = J_a e^{i(\omega t - kz)} \quad (1)$$

$\omega = 2\pi f$ ,  $f$  is the frequency of the excitation current,  $k = \pi / \tau$ ,  $\tau$  is the pole pitch, and  $J_a = 3\sqrt{2}kNI / p\tau$ .

An analytic model of the EM phenomena occurring in the TC-1 pump was developed according to Cho and Hong [12]. The model used a combination of the separation of variables method and Fourier transformations to obtain integral formulations of the magnetic vector potential, and the r- and z-components of the magnetic flux density. These integrals were evaluated using numerical integration to yield values of the vector potential and the magnetic flux density at specific points in the calculation domain. The time-averaged EM body forces, power density and pump efficiency were then calculated from the vector potential and magnetic flux density.

Since the source current in the inductor coils has a component only in the  $\theta$ -direction and is varying sinusoidally in time, the magnetic vector potential has the form:

$$\vec{A} = \vec{A}(r, z, t) = A_\theta(r, z) \cdot e^{i\omega t} \quad (2)$$

with only a component in the  $\theta$ -direction and also varying sinusoidally in time. For the general case of an electrically conducting fluid moving with a velocity  $\vec{v}$  in a magnetic field, the magnetic vector potential distribution is governed by the following equation:

$$-\nabla^2 A = \mu\sigma \left( -\frac{\partial \vec{A}}{\partial t} + \vec{v} \times (\nabla \times \vec{A}) \right) \quad (3)$$

where  $\mu$  is the magnetic permeability and  $\sigma$  is the electrical conductivity of the medium. By applying the separation of variables method and Fourier transformations (Cho and Hong [12]), we can obtain the expression of vector potential as

$$A(r, z) = \frac{i\mu J_a}{2\pi} \int_{-\infty}^{\infty} \frac{e^{-i(\zeta+k)L} - 1}{\zeta + k} \frac{G(r, \zeta)}{\alpha(\zeta)H(\zeta)} e^{i\zeta z} d\zeta \quad (4)$$

where:

$$G(r, \zeta) = K_0(\alpha_2 r_1) I_1(\alpha_2 r) + I_0(\alpha_2 r_1) K_1(\alpha_2 r) \quad (5)$$

$$H(\zeta) = K_0(\alpha_2 r_1) I_0(\alpha_2 r_2) - I_0(\alpha_2 r_1) K_0(\alpha_2 r_2) \quad (6)$$

Expressions for the two components of the magnetic flux density are:

$$B_r(r, z) = \frac{\mu J_a}{2\pi} \int_{-\infty}^{\infty} \frac{e^{-i(\zeta+k)L} - 1}{\zeta + k} \frac{G(r, \zeta)}{\alpha(\zeta)H(\zeta)} (\zeta e^{i\zeta z}) d\zeta \quad (7)$$

$$B_z(r, z) = \frac{i\mu J_a}{2\pi} \int_{-\infty}^{\infty} \frac{e^{-i(\zeta+k)L} - 1}{\zeta + k} \frac{e^{i\zeta z} P(r, \zeta)}{\alpha(\zeta)H(\zeta)} d\zeta \quad (8)$$

where:

$$P(r, \zeta) = \alpha [K_0(\alpha r_1) I_0(\alpha r) - I_0(\alpha r_1) K_0(\alpha r)] \quad (9)$$

The integrals in equations 4, 7 and 8 can be evaluated using either the residue theorem (ref) or via numerical integration techniques. Equations 4, 7 and 8 are used to calculate the components of the time-averaged EM body forces,  $\vec{F}$ , the power density,  $p$ , and pump efficiency,  $\eta$ . These are calculated from the vector potential and magnetic flux density by the following expressions:

$$\vec{F} = \vec{J} \times \vec{B} \quad (10)$$

$$F_z = \frac{1}{2} \text{Re}[\sigma(i\omega A - vB_r) \cdot B_r^*] \quad (11)$$

$$F_r = \frac{1}{2} \text{Re}[\sigma(i\omega A - vB_r) \cdot B_z^*] \quad (12)$$

$$p = \frac{1}{2} \text{Re}[\vec{J} \cdot \vec{E}^*] = \frac{1}{2} \text{Re}[\sigma(i\omega A - vB_r) \cdot (i\omega A^*)] \quad (13)$$

$$\eta = \frac{\int_0^L \int_{r_1}^{r_2} F_z r dr dz}{\int_0^L \int_{r_1}^{r_2} p r dr dz} \quad (14)$$

## NUMERICAL MODELING

The numerical solutions have been obtained using the software package FEMLAB (Comsol, Sweden). It is a MATLAB-based platform and relies on the finite element method (FEM) to discretise and solve the partial differential equations. The software can run the finite element analysis together with adaptive meshing and error control according to a variety of iterative numerical solvers. The applicability, validity and robustness of the code have been addressed by a number of previous authors [13,14].

In this work, we use the azimuthal induction currents and vector potential application mode of FEMLAB for axially symmetric 2 D simulation based on given equivalent current sheet in the angular direction. The problem is formulated using the only nonzero component of the magnetic vector potential, in the azimuthal component. For present modeling, with currents having only one nonzero component the magnetic potential is used. The parameters of the TC-1 pump for calculation are used:  $\omega = 120\pi$  rad s<sup>-1</sup>, fluid velocity  $v = 1$  m s<sup>-1</sup>, inner core radius  $r_1 = 0.0295$  m, outer core radius  $r_2 = 0.038$  m,  $L = 0.653$  m, the pole pitch  $\tau = 0.105$  m,  $J_a = 30000$  A/m,  $\mu = 4\pi \times 10^{-7}$  N s<sup>2</sup> C<sup>-2</sup>,  $\sigma = 1.04 \times 10^7$   $\Omega^{-1} m^{-1}$ .

## RESULTS AND DISCUSSION

Fig.2 and Fig.3 shows the radial and axial components of the magnetic flux density in the TC-1 pump along the pump axis Z. Here, we give the comparison of numerical results and theoretical solution. Both of the real and imaginary parts are illustrated. As shown in the Figures, good agreement can be found. Comparing with the axial component, considerable end effects on the radial component of the magnetic flux density occurs at both of the entrance and exit of the pump. Witness that the axial magnetic flux density is one order less than the radial component. Fig.4 shows the magnetic flux density vector graph from the numerical data for TC-1 pump.

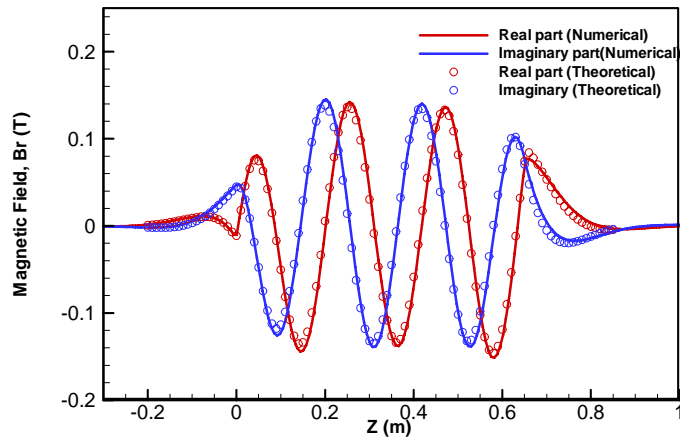


Fig.2 Radial component of the magnetic flux density in the TC-1 pump along the pump axis Z.

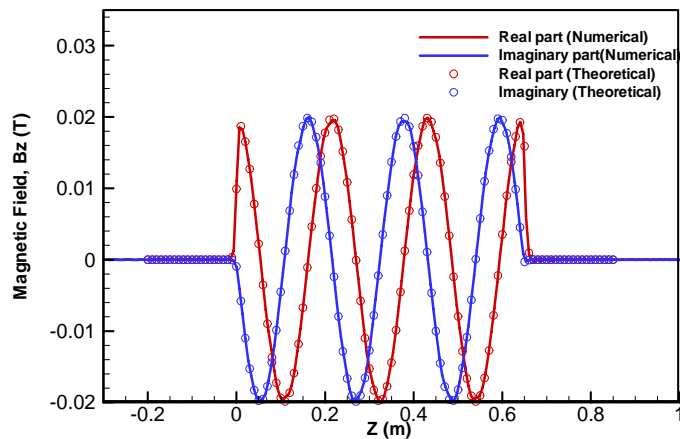


Fig.3 Axial component of the magnetic flux density in the TC-1 pump along the pump axis Z.

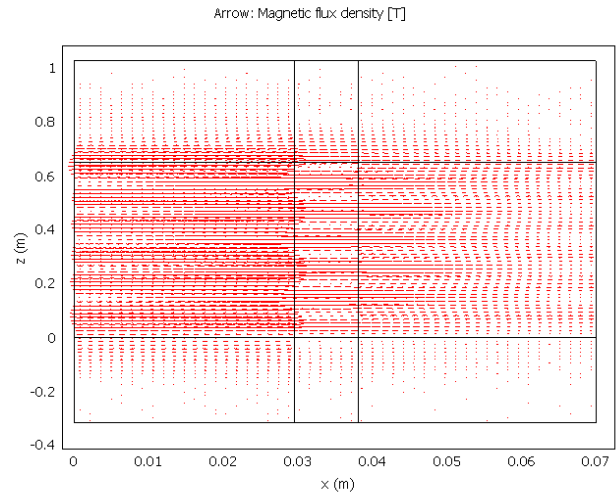


Fig. 4 Magnetic flux density vector graph from the numerical data for TC-1 pump.

Fig. 5 shows the magnetic vector potential in the TC-1 pump along the pump axis Z. As shown in Fig. 5, there exist little difference in the entrance and exit of the pump while the data coincide with each other inside the pump. The reason is that the permeability of the iron core has been assumed to be infinite in obtaining closed-form solutions in Cho and Hong's theoretical model. Fig.6 shows the distribution of magnetic vector potential from the numerical data for TC-1 pump. The force density distribution and power distribution, which are calculated through Eq.(11) and Eq. (13), in TC-1 pump are illustrated in Fig.7 and Fig.8. While in both cases the curves are relative constant through the length of the pump, end effects are apparent. These end effects have a significant negative effect on overall pump efficiency

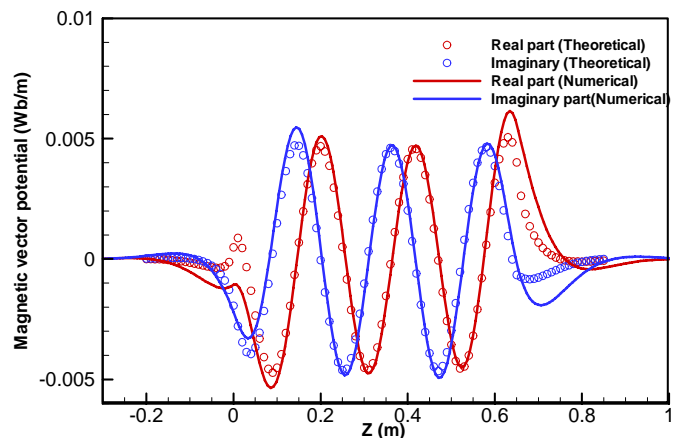


Fig.5 Magnetic vector potential in the TC-1 pump along the pump axis Z.

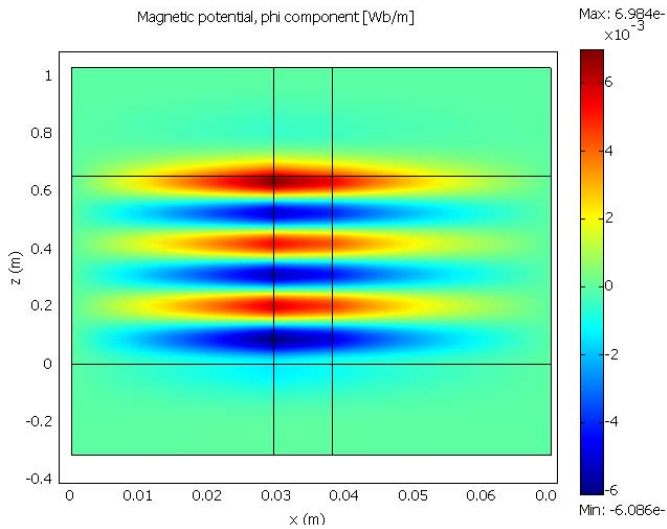


Fig. 6 Distribution of magnetic vector potential from the numerical data for TC-1 pump

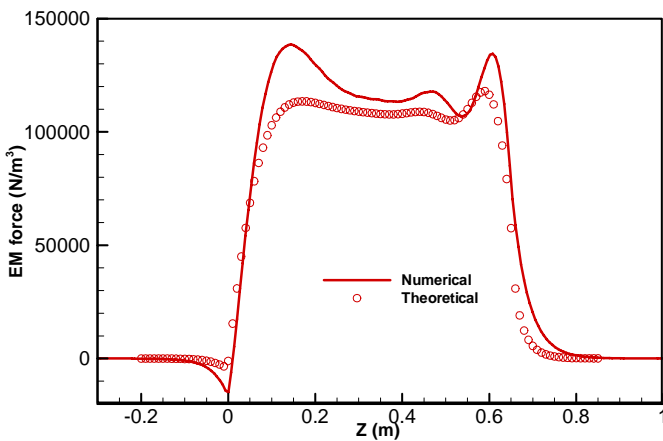


Fig.7 Force density distribution in TC-1 pump

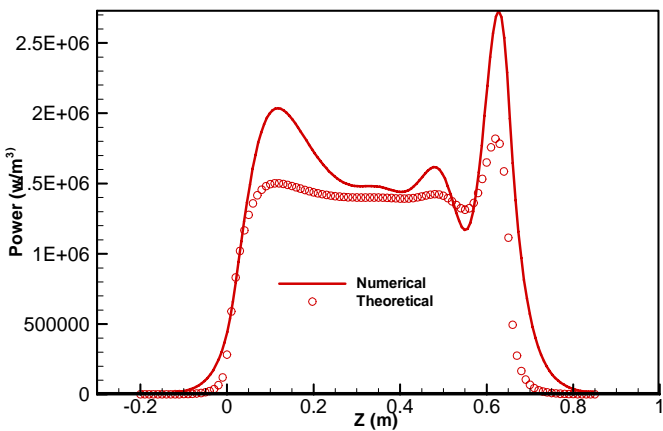


Fig. 8 Power density distribution in the TC-1 pump.

## CONCLUSIONS

The initial step on modeling the pilot molten lead-bismuth target circuit (TC-1 annular linear induction pump at the University of Nevada, Las Vegas (UNLV) have been made. Both theoretical and numerical methods based on the equivalent current sheet assumption were used to explore the characteristics of the TC-1 EM pump and give insight into future EM pump design. The EM body forces were calculated using both simplified analytic expressions, as well as by numerical solution of Maxwell's equation. Since the present study is the initial step on modeling of EM pump, our present work only limit on simple model. The hydraulic effect was not considered in current model and also the magnetic field was calculated only by simply applying equivalent current sheet model while the magnetic fields in the real system will be much more complicated. All of these factors will be coupled in the future work.

## ACKNOWLEDGMENTS

The authors would like to thank the financial support from the DOE Transmutation Research Program.

## REFERENCES

- [1] Leslie R. Dahl, 2000, "Electromagnetic pump", in AccessScience @ McGraw-Hill, <http://www.accessscience.com>, DOI 10.1036/1097-8542.222600, last modified: April 10.
- [2] R. S. Baker, and M. J. Tessier, 1987 "Handbook of Electromagnetic Pump Technology", Elsevier Science Publishing Co., Inc.
- [3] D. Rinderknecht, A. I. Hicherson and M. Gharib, 2005, "A valveless micro impedance pump driven by electromagnetic actuation", Journal of Micromechanics and Microengineering, **15**, 861-866.
- [4] N.T. Nguyen, X.Y. Huang, 2002, "MEMS-Micropumps: A Review, Journal of Fluids Engineering", **124**, 384-392.
- [5] I. Boldea, S. A. Nasar, 2001, "The Induction Handbook", CRC press, Chapter 2.
- [6] J. Ma, N. Li, S. Ignatiev and V. Kutanov, 2006, "Performance of Magnetic Hydro-Dynamic Pump in Lead-Bismuth Eutectic Target Circuit (TC-1)", International Congress on Advances in Nuclear Power Plants, Reno, NV USA, June 4-8.
- [7] R. Stieglitz, 2003, "MHD-features of the Main Service and Bypass Pump in the MEGAPIE Design", Forschungszentrum Karlsruhe GmbH report.
- [8] H. Araseki, I. R. Kirillov, G. V. Preslitsky, and A. P. Ogorodnikov, 2000, "Double-supply-frequency Pressure Pulsation in Annular Linear Induction Pump, Part I: Measurement and Numerical Analysis", Nuclear Engineering and Design, **195**, 85-100.

[9] R. Stieglitz, and J. Zeininger, 2005, "A 2D Model to Design MHD Induction Pumps", The 15<sup>th</sup> Riga and 6<sup>th</sup> Pamir Conference on Fundamental and Applied MHD, Latvia, June 27-July 1, 35-49.

[10] H. Araseki, I. R. Kirillov, G. V. Preslitsky, A. P. Ogorodnikov, 2006, "Magnetohydrodynamic Instability in Annular Linear Induction Pump, Part II, Suppression of Instability by Phase Shift", Nuclear Engineering and Design, **236 (9)**, 965-974.

[11] I. R. Kirillov, D. M. Obukhov, 2003, "Two Dimensional Model for Analysis of Cylindrical Linear Induction Pump Characteristics: Model Description and Numerical Analysis", Energy Conversion and Management, **44**, 2687-2697.

[12] S. Cho, S.H. Hong, 1998, "The magnetic field and performance calculations for an electromagnetic pump of a

liquid metal", Journal of physics, D: Applied Physics, **31**, 2754-2759.

[13] U. Shavit, G. Bar-Yosef, R. Rosenzweig, S. Assouline, 2002, "Modified Brinkman equation for a free flow problem at the interface of porous surfaces: The Cantor-Taylor brush configuration case", Water Resour. Res. **38** 325-321.

[14] U. Shavit, R. Rosenzweig, S. Assouline, 2004, "Free flow at the interface of porous surfaces: a generalization of the Taylor brush configuration," Transport. Porous Med. **54**, 345-353.